Controlled Synthesis of Metal-Insulator-Metal Nanoparticles for Enhanced Raman Spectroscopy

Junhu Zhou[1], Xin Qi[2*], John X.J. Zhang[1*]

1 Thayer School of Engineering, Dartmouth College, Hanover, NH 03755, USA
2 Department of Chemistry, Dartmouth College, Hanover, NH 03755, USA
*Corresponding author: Xin.Qi@dartmouth.edu, John.Zhang@Dartmouth.edu

COMSOL Multiphysics® Simulations

FEA simulations were performed using COMSOL Multiphysics® (version 6.2) to solve Maxwell's wave equations for the scattered electric field (E_{sc}) using the Wave Optics module. The governing equation is given by[1]:

$$\nabla \times \mu_r^{-1}(\nabla \times \boldsymbol{E_{sc}}) - {k_0}^2\left(\epsilon_r - \frac{j\sigma}{\omega\epsilon_0}\right)\boldsymbol{E_{sc}} = 0 \qquad (S1)$$

where k_0 is the wavenumber in free space, μ_r is the relative permeability, ϵ_r is the relative permittivity, and σ is the conductivity of the material.

A three-dimensional (3D) MIM nanoparticle model was constructed to evaluate the electric field distribution and compute the absorption, scattering, and extinction cross-sections of the nanoparticle in an aqueous environment. The absorption cross-section (σ_{abs}) is defined as:

$$\sigma_{abs} = \frac{1}{I_0}\iiint Q dV \qquad (S2)$$

where Q represents the power loss density within the MIM nanoparticle, and the integral is taken over its entire volume. Here, I_0 denotes the incident light intensity.

The scattering cross-section (σ_{sc}) is defined as:

$$\sigma_{sc} = \frac{1}{I_0}\iint (\boldsymbol{n}\cdot\boldsymbol{S_{sc}})dS \qquad (S3)$$

where $\boldsymbol{n}$ is the unit normal vector pointing outward from the nanoparticle, and $\boldsymbol{S_{sc}}$ is the scattered Poynting vector. The integral is computed over the entire closed surface of the nanoparticle. The extinction cross-section is determined as the sum of the absorption and scattering cross-sections.

The parameters used in the COMSOL simulations are summarized in **Table S1**. Depending on the geometry complexity and mesh density, the computational time ranged from 7 to 17 hours.

Colloidal Forces Calculation

As described in Eqs. 1–3 of the main text, we employ a mean-field approach to estimate the long-range interactions between silica-coated AuNPs and exterior AuNPs in an aqueous solution. These interactions consist of an attractive van der Waals (vdW) potential, $W(r)$, and an electrostatic repulsion term, $V(r)$.

For vdW interactions, the Hamaker constants used in our calculations are $A_1 = 1.35 \times 10^{-19}\,J$ for Au and $A_2 = 1.02 \times 10^{-20}\,J$ for SiO_2. The effective Hamaker constant for the gold-silica system ($1.34 \times 10^{-19}\,J$) is calculated using the averaging rule[2]:

$$A_{12} = \sqrt{A_1 A_2} \quad (S4)$$

Electrostatic repulsion between charged particles in an ionic solution arises from the formation of an electric double layer at the interface between SiO_2, Au surfaces, and the surrounding medium. This interaction is described using the linearized Poisson-Boltzmann equation, which is valid under the assumption of low surface potential and low ionic strength:

$$\nabla^2\psi - \kappa^2\psi = 0 \quad (S5)$$

Here, ∇ is the Laplacian operator, ψ is the potential at the nanoparticle surface, and κ is the Debye screening parameter. By applying the Derjaguin approximation along with appropriate boundary conditions, Eq. 3 in the main text provides an analytical expression for the electrostatic interaction between two similarly sized charged spheres at any separation[3]. Notably, this formulation requires evaluating ψ strictly at the nanoparticle surface rather than using the commonly adopted zeta potential. The absolute surface potential, until recently, has been challenging to measure directly.

Accurate measurement of absolute surface potential has historically been challenging. However, it can be determined indirectly by solving the modified Grahame equation (Eqs. 5 and 6 in the main text) using a known surface charge density q. The surface charge density of AuNPs is estimated based on the surface ligand density of borohydride and citrate, while the charge density of APTES-treated SiO_2 surfaces is derived from the ionization rate of silanol groups and the surface coverage of APTES. The specific values used in our calculations are summarized in **Table S2**.

Enhancement Factor Calculation

The enhancement factor of SERS can be obtained by the following equation:

$$(Enhancement\ factor) = \frac{\left(\frac{I_{SERS}}{N_{SERS}}\right)}{\left(\frac{I_{NR}}{N_{NR}}\right)} \quad (S6)$$

where I_{SERS} and I_{NR} are the intensities of SERS and normal Raman (Figure S6), respectively, and N_{SERS} and N_{NR} are their numbers of Raman-scattering molecules present in light collection volume.

N_{NR} can be calculated by using the molecular weight (M_{4-NTP}) and density (d_{4-NTP}) of 4-NTP and estimating the collection volume f the sample. The collection volume was defined as a cylinder of 1.5 μm ($= 1.22 \times 0.633\,\mu m/0.5$) diameter and 6 μm height from the measured beam size:

$$N_{NR} = \frac{N_A \times V_{focal} \times d_{4-NTP}}{M_{4-NTP}} \quad (S7)$$

$$= \frac{(\pi \times 0.75^2 \times 6) \times 10^{-12} \times 1.362 \times (6.02 \times 10^{23})}{155.17} = 5.6 \times 10^{10}$$

I_{NR} of 4-NTP at 1335 cm^{-1} was obtained as 347.5 ± 79.8 from 5 times measurement, where 633 nm and $\times 50$ objective lens were used, and acquisition time was 0.5 s. N_{SERS} was defined as the number of molecules absorbed on the surface of MIM nanoparticles, which is approximately estimated using the area occupied by one molecule. It is worth noting that it is the maximum value that can be attained by full surface coverage. The active hotspot areas of

MIM nanoparticle is estimated as $1.38 \times 10^4\ nm^2$ ($52 \times 4\pi \times 6.5^2 \times 0.5$). The molecular projected area of MB is $\sim 0.34\ nm^2$, as estimated[4]. Therefore, N_{SERS} for MIM nanoparticle is estimated as 4.06×10^3.

Then, the EF value of MIM nanoparticle and 120 nm AuNP are calculated as follow:

$$EF_{MIM} = \frac{\frac{I_{SERS}}{N_{SERS}}}{\frac{I_{NR}}{N_{NR}}} = \frac{\frac{3421.4 \pm 184.9}{4.06 \times 10^3}}{\left(\frac{347.5 \pm 79.8}{35.6 \times 10^{10}}\right)} = (8.63 \pm 2.04) \times 10^8$$

Table S1. Parameters in COMSOL Multiphysics® Simulations

Name	Expression	Value	Description
w	950[nm]	9.5E-7 m	Width of physical geometry
t_pml	150[nm]	1.5E-7 m	PML thickness
phi	pi/2	1.5708	Azimuthal angle of incidence
theta	0	0	Polar angle of incidence in water
I0	1[MW/m^2]	1E6 W/m^2	Intensity of incident field
P	I0*w^2*cos(theta)	9.025E-7 W	Port power
R0	126[nm]/2	6.52E-8 m	Radius of silica sphere
R1	120[nm]/2	6E-8 m	Radius of core gold sphere
r0	13[nm]/2	6.5E-9 m	Radius of exterior sphere
D0	25[nm]	2.5E-8 m	Separation of exterior spheres

Table S2. Parameters in colloidal forces calculation

Name	Value	Source
AuNP radius	6.5 nm	Input
SiO_2 radius	64 nm	Input
Silanol group density	4.7 per nm^2	ref[5]
Silanol group ionization at pH 7	0.6 per nm^2	ref[5]
APTES coverage	3 per nm^2	ref[6]
BH_4^- coverage	1.5 per nm^2	ref[7]
Citrate coverage	1 per nm^2	ref[8]
AuNP surface charge density with BH_4^-	0.24 C m^{-2}	Calculation
AuNP surface charge density with citrate	0.48 C m^{-2}	Calculation
SiO_2 surface charge density with APTES	-0.096 C m^{-2}	Calculation
AuNP surface potential with BH_4^-	-40 mV	Calculation
AuNP surface potential with citrate	-310 mV	Calculation
SiO_2 surface potential with APTES	170 mV	Calculation

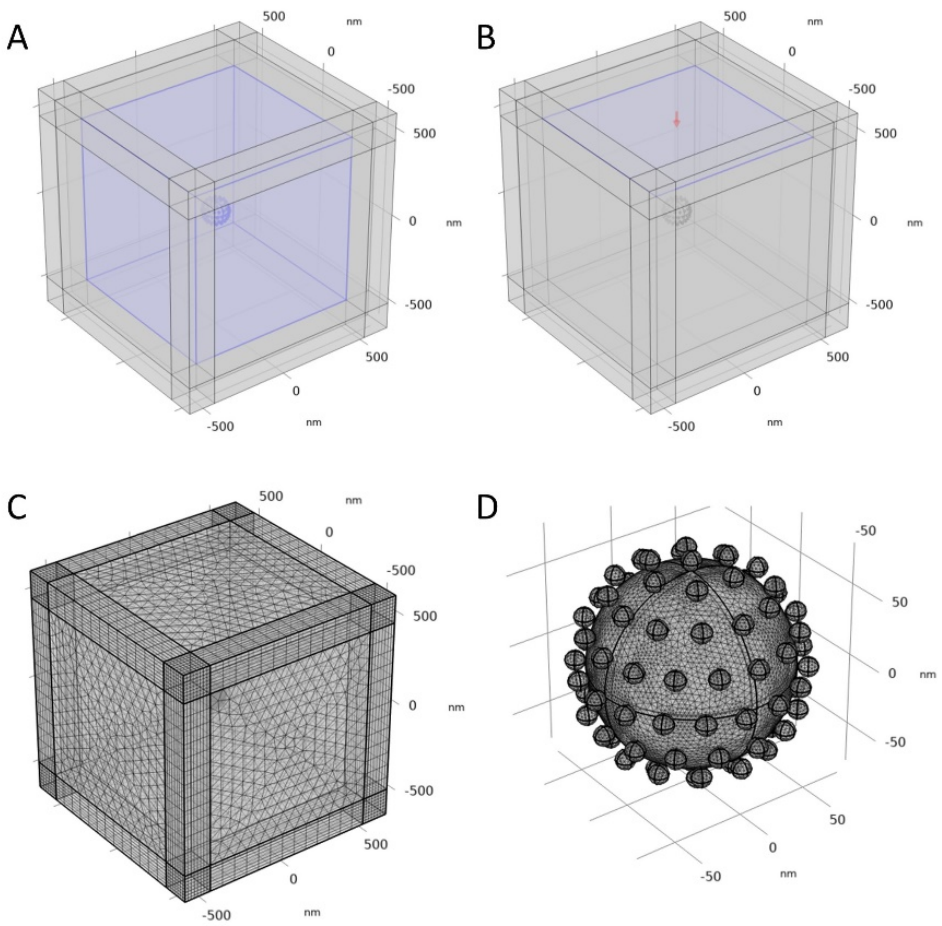

Figure S1. Geometry and mesh of the COMSOL Multiphysics® Simulations model used in this research. (A) The 3D geometry of the MIM nanoparticle. The blue region is selected as physical domain. The remaining elements are perfectly matched layer. (B) Incident light entering port the simulation domain. (C) The meshing scheme under physics-controlled method. (D) The detailed meshing of the MIM nanoparticle.

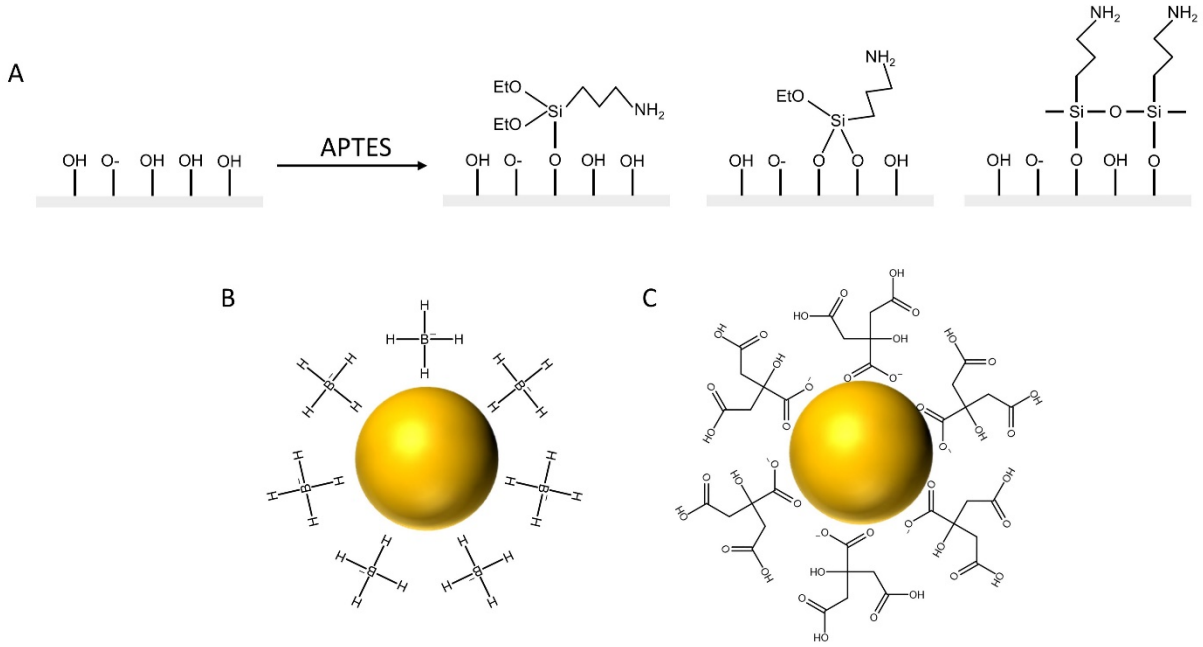

Figure S2. Schematic representation of surface ligands functionalized nanoparticle surfaces. (A) APTES functionalization of silica surface and possible orientations of the APTES molecule attached to the silanol-terminated surface through the silanization reaction. (B) Schematic illustration of sodium borohydride stabilized AuNP. (C) Schematic illustration of sodium citrate stabilized AuNP.

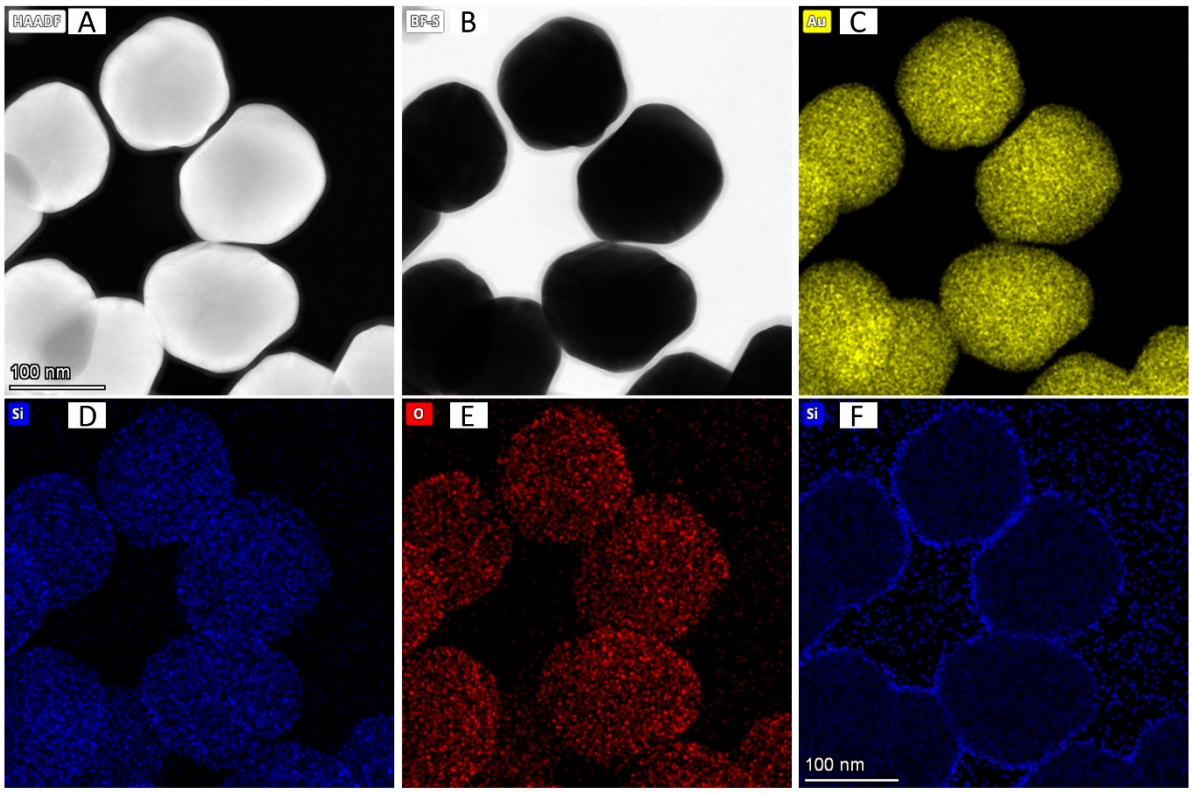

Figure S3. TEM and EDS characterization of silica-coated AuNPs. (A) High-angle annular dark-field (HAADF) TEM image of silica-coated AuNPs. (B) Bright field TEM image of silica-coated AuNPs. EDS elemental mapping of the silica-coated AuNPs, including (C) Au element, (D) Si element, and (E) O element. (F) EDS elemental mapping of the Si element, filtered by the Au element.

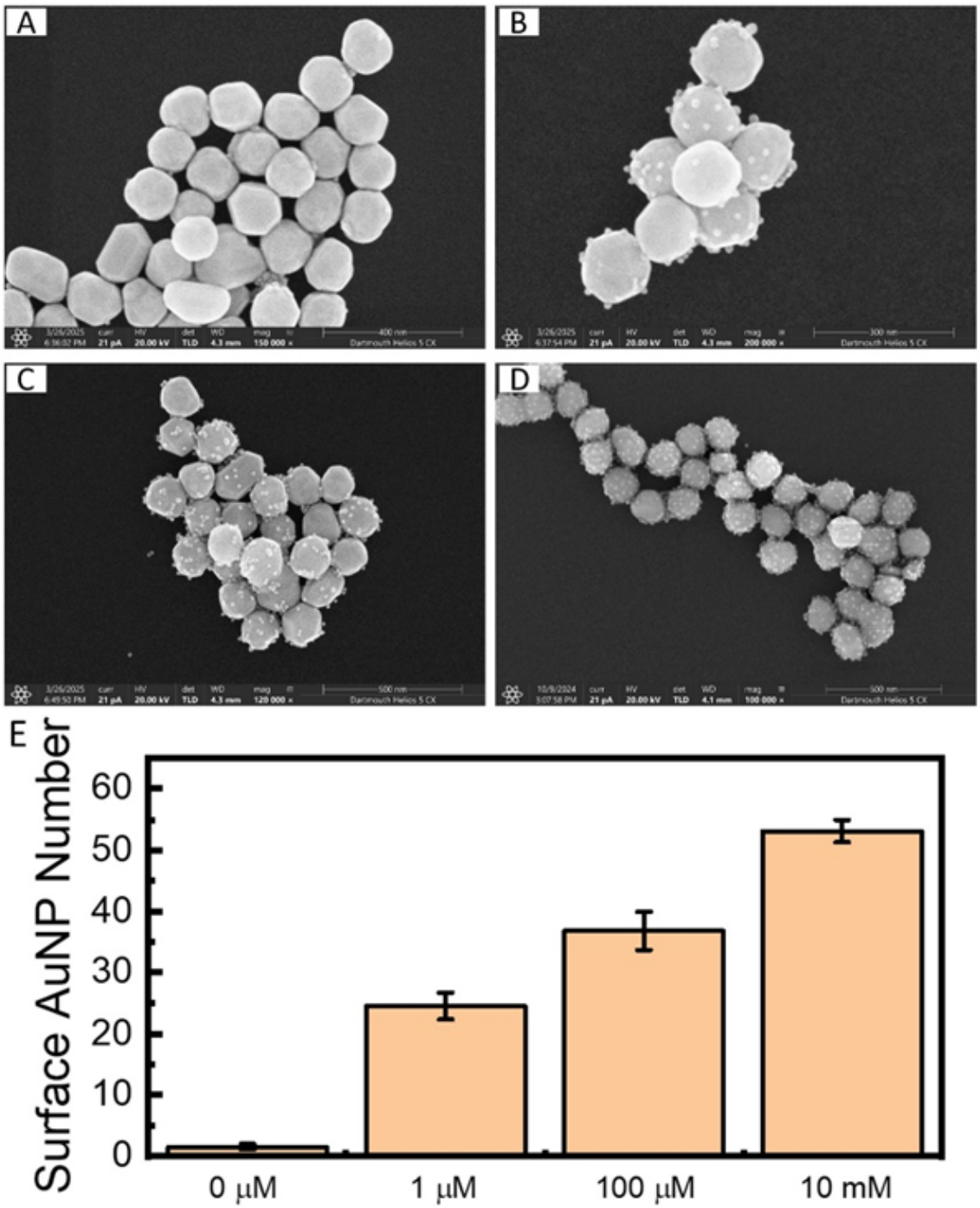

Figure S4. Assembly of MIM nanoparticles with different APTES concentration. SEM images of MIM nanoparticles treated with 0 (A), 1 μM (B), 100 μM (c) and 10 mM (D) APTES treatment on silica shell. (E) The number of AuNPs attracted to the silica surface in different APTES treatment groups.

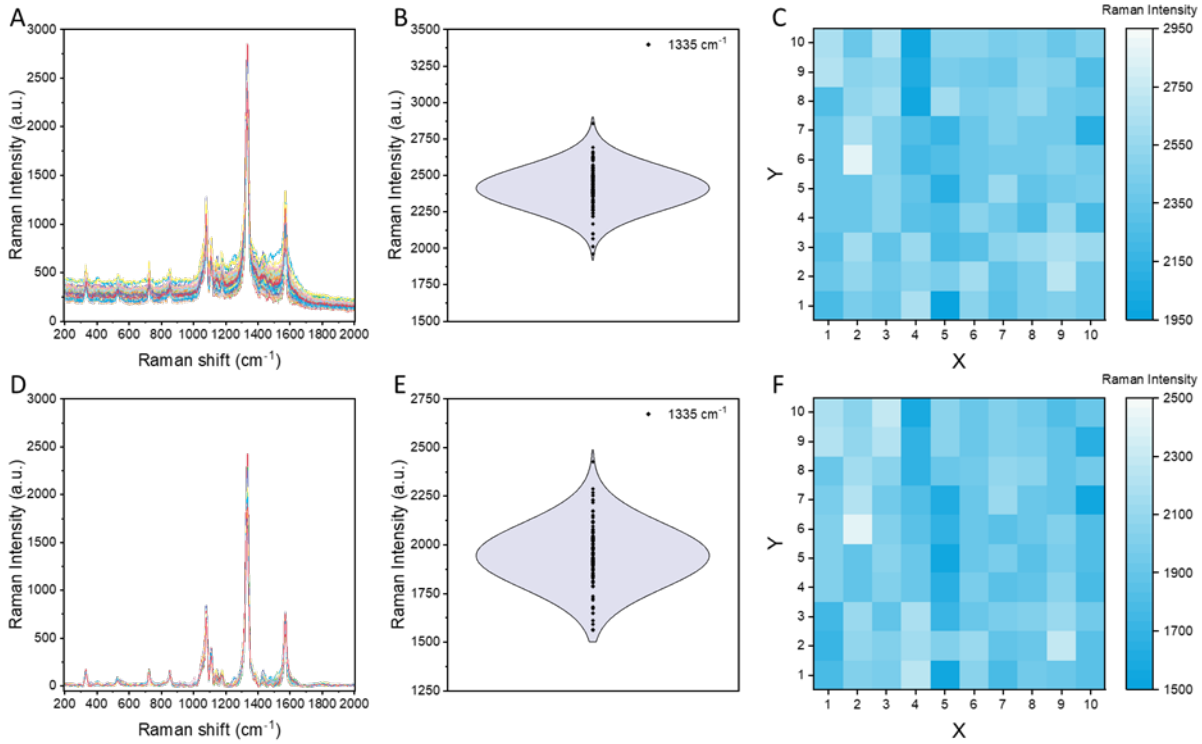

Figure S5. SERS analysis of 4-NTP. (A) Raw SERS spectra of 4-NTP collected from 100 individual measurements. (B) Violin plot with Normal distribution curve showing the distribution of Raman intensities at 1335 cm^{-1}. (C) Heatmap illustrating spatial variation of Raman intensity at 1335 cm^{-1}. (D–F) Corresponding results after baseline correction, including corrected spectra (D), updated violin plot (E), and adjusted heatmap (F).

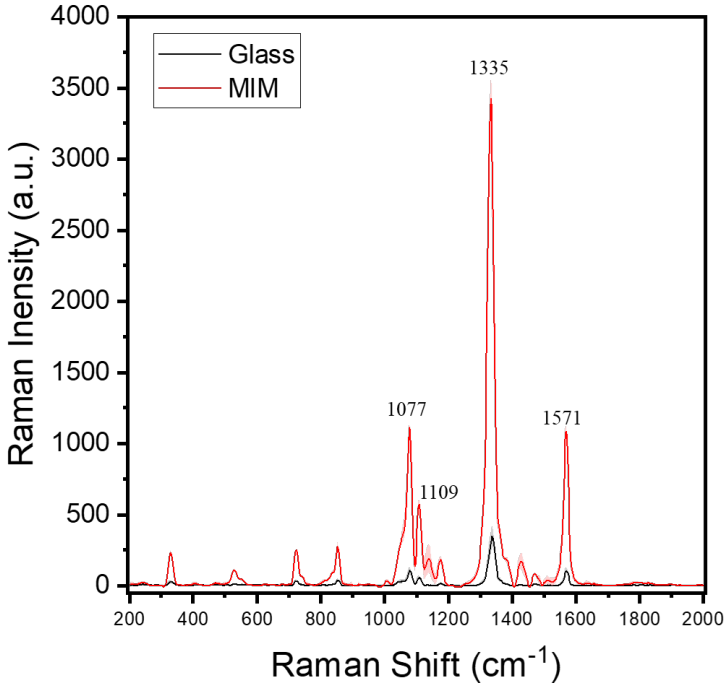

Figure S6. SERS spectra of 4-NTP measured on different substrates. Shaded regions indicate the standard deviation from five measurements, reflecting signal reproducibility

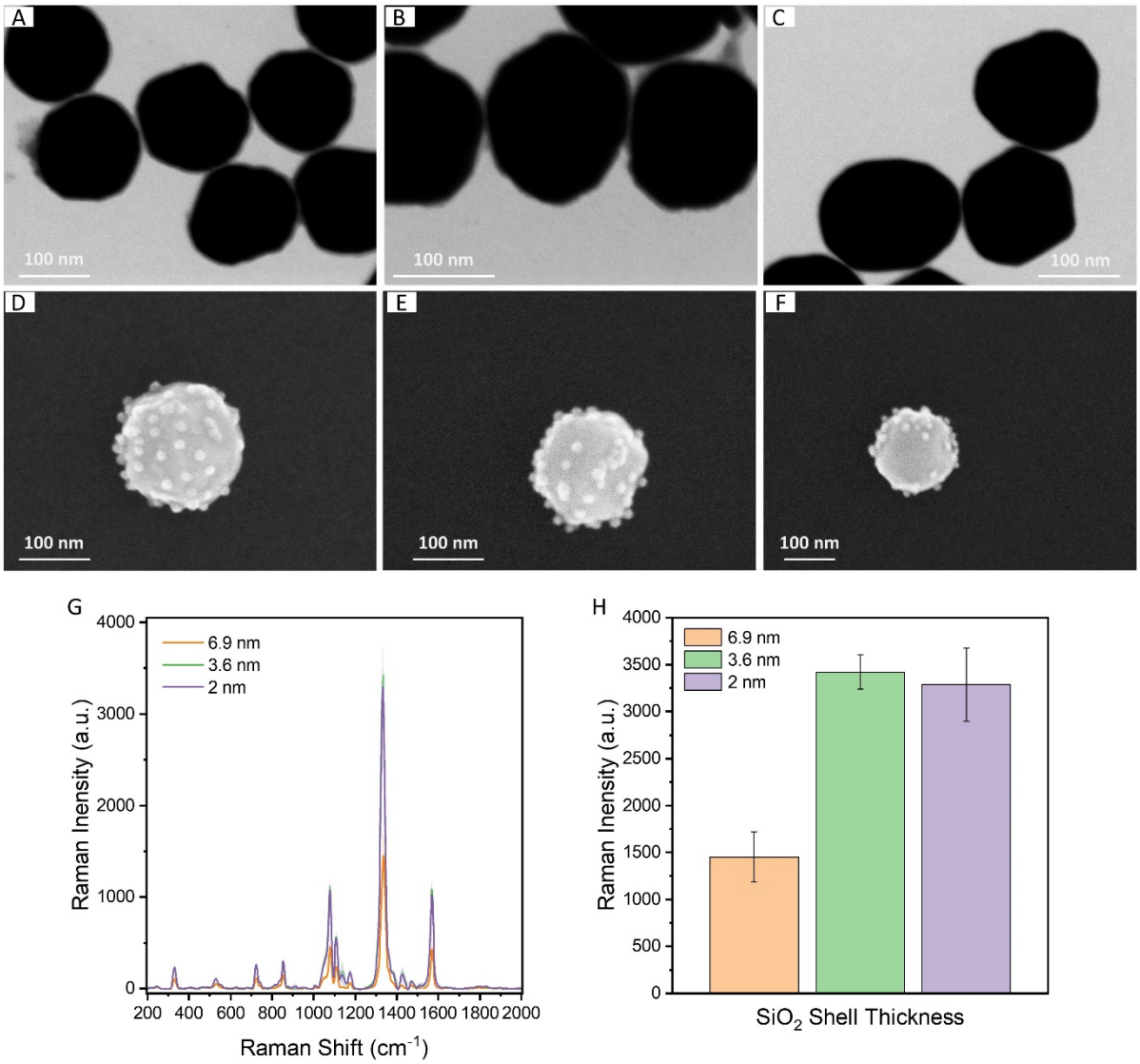

Figure S7. MIM nanoparticles with varying silica shell thicknesses and their corresponding SERS performance. (A-C) STEM images of Au@SiO_2 nanoparticles with silica shell thicknesses of 6.9 nm, 3.6 nm, and ~2 nm, respectively. (D-F) SEM images of fully assembled MIM nanoparticles using the same corresponding shell thicknesses. (G) SERS spectra of 4-NTP measured using the three types of MIM nanoparticles. (H) Comparison of Raman intensity at 1335 cm^{-1} for each MIM configuration, highlighting the influence of shell thickness on SERS enhancement.

References:

1 R. K. Saini, A. Kumar, V. Goyal, A. Agarwal and R. Prajesh, *Mater Today Proc*, 2023, **76**, 383–387.

2 M. Götzinger and W. Peukert, *Langmuir*, 2004, **20**, 5298–5303.

3 J. E. Sader, S. L. Carnie and D. Y. C. Chan, *J Colloid Interface Sci*, 1995, **171**, 46–54.

4 H. Tsutsumi, S. Furumoto, M. Morita and Y. Matsuda, *J Colloid Interface Sci*, 1995, **171**, 505–511.

5 F. S. Emami, V. Puddu, R. J. Berry, V. Varshney, S. V. Patwardhan, C. C. Perry and H. Heinz, *Chemistry of Materials*, 2014, **26**, 2647–2658.

6 D. Meroni, L. Lo Presti, G. Di Liberto, M. Ceotto, R. G. Acres, K. C. Prince, R. Bellani, G. Soliveri and S. Ardizzone, *The Journal of Physical Chemistry C*, 2017, **121**, 430–440.

7 A. Akça, A. E. Genç and B. Kutlu, *Appl Surf Sci*, 2019, **473**, 681–692.

8 G. Chong, E. D. Laudadio, M. Wu, C. J. Murphy, R. J. Hamers and R. Hernandez, *The Journal of Physical Chemistry C*, 2018, **122**, 28393–28404.